CHEMISTRY OF MATERIALS

ARTICLE

pubs.acs.org/cm

Beyond the Limits of X-ray Powder Diffraction: Description of the Nonperiodic Subnetworks in Aluminophosphate-Cloverite by NMR Crystallography

Charlotte Martineau,*[,‡] Boris Bouchevreau,[‡] Zhijian Tian,[§] Sven-Jare Lohmeier,[∥] Peter Behrens,[∥] and Francis Taulelle[‡]

[‡]Tectospin — Institut Lavoisier de Versailles, CNRS UMR 8180, Université de Versailles Saint-Quentin en Yvelines, 45 avenue des États-Unis, 78035 Versailles Cedex, France

[§]State Key Laboratory of Catalysis, Dalian National Laboratory for Clean Energy, Dalian Institute of Chemical Physics, Dalian 116023, China

[∥]Institut für Anorganische Chemie, Leibniz Universität Hannover, Callinstrasse 9, D-30167 Hannover, Germany

Supporting Information

ABSTRACT: NMR crystallography of the fluorinated aluminophosphate cloverite is presented, with an emphasis on the description of the nonperiodic part of the compound, i.e., the fluorine and organic subnetworks, which are very difficult to access by usual X-ray powder diffraction methods. Multinuclear high-resolution 1D ^{27}Al and ^{31}P NMR support the main cloverite-type topological features previously proposed for aluminum cloverite from powder X-ray diffraction. Spatial proximities are extracted from the 2D ^{31}P−^{31}P and ^{27}Al−^{31}P NMR spectra, allowing a full assignment of the ^{31}P and ^{27}Al resonances to the corresponding phosphorus and aluminum sites in the structure. To go further into the description of the main periodic framework, ^{13}C, ^{15}N, and ^{1}H 1D and ^{1}H−^{1}H and ^{1}H−^{31}P 2D NMR measurements are employed, allowing the characterization and selective locations of the two costructural-directing agents in the pores and channels of the framework. The nonperiodic fluorine subnetwork is described by means of ^{19}F-X (X = ^{27}Al and ^{31}P) 2D NMR experiments. Two kinds of fluorine atoms are distinguished: F^- ions trapped in *D4R* units and F atoms covalently bonded to terminal Al or P atoms and which interrupt the AlPO network. Through the example of aluminum cloverite, we show that, despite the considerable complexity of such systems, an extremely detailed structural model can be obtained, including the simple rules that allow the description of the nonperiodic subnetworks that tailor the structure and properties of a compound, by coupling powder X-ray diffraction and high-resolution NMR data in a generalized crystallography approach.

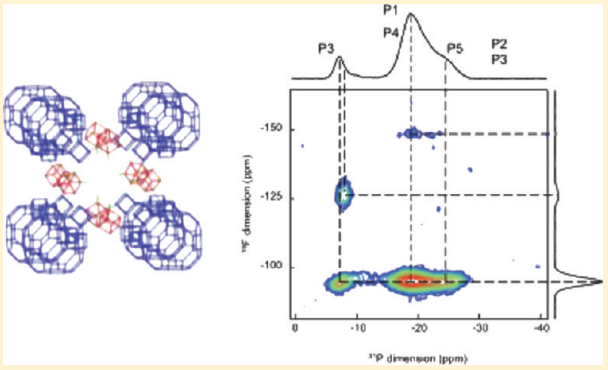

KEYWORDS: NMR crystallography, generalized crystallography, cloverite, fluorinated aluminophosphate, high-resolution NMR, 2D correlation

1. INTRODUCTION

Since their discovery in the early 1980s,[1,2] aluminophosphates have received much attention because of their potential applications as molecular sieves in absorption, separation, or shape-selective catalysis.[3−7] The cloverite-type (-CLO)[8] framework, initially obtained with gallium atoms,[9] is a fluorinated molecular sieve with extra-large pores of 20-ring-openings, making this framework one with the lowest density among the approved zeolites framework types.[10] Recently, Y. Wei et al.[11] obtained the equivalent topology with aluminum atoms, referred to in their work as DNL-1 (Dalian National Laboratory Number 1), of chemical formula $|(C_6N_2H_{88})_{104}$ - $(C_6N_2H_{11})_{80}$ $(H_2O)_{910}|$ $[Al_{768}P_{768}O_{2976}(OH)_{192}$ $F_{288}]$, through ionothermal synthesis using two amines (and not only one as in the case of gallium cloverite) as costructure-directing agents (co-SDAs). In addition to high surface area and micropore volume, DNL-1 also shows excellent stability compared to the gallium cloverite.[11] S. J. Lohmeier et al. were able to crystallize a similar aluminum cloverite compound, LUH-2 (Leibniz Universität Hannover Number 2), from another ionic liquid containing mixed anions. The structural topology of DNL-1 was confirmed by Rietveld refinement from powder X-ray diffraction (PXRD) data and ^{31}P, ^{19}F, ^{13}C, and ^{27}Al one-dimensional (1D) solid-state nuclear magnetic resonance (NMR) to be analogous to that of the gallium cloverite. The 1D ^{31}P and ^{27}Al NMR results on DNL-1[11] indicated the presence of P−OH and Al−OH groups, while

Received: July 22, 2011
Revised: September 23, 2011
Published: October 11, 2011

the ^{19}F NMR data showed the presence of F^- ions trapped in every double 4-rings (*D4R*) cages of the structure as well as the presence of terminal Al−F bonds. However, the NMR study was restricted to 1D NMR spectra, which limits the amount of local structural details that can be extracted. Increasing the degree of accuracy in the structural description of these materials is probably an essential further step to better understand and tailor their exceptional properties.

Because solid-state nuclear magnetic resonance (NMR) spectroscopy is atom specific and sensitive to the local order around a given nucleus, this technique has gradually become an essential tool to assist the structural resolution and description of solids by diffraction. Combination of diffraction and NMR data for powders in a so-called SMARTER approach (structure elucidation by combining magnetic resonance, computation modeling, and diffractions) is of particular importance for crystalline aluminophosphates potentially lacking long-range order because, for example, of the presence of organic templates or of local and random distributions of isoelectronic atoms or group of atoms (e.g., OH/F...) which cannot easily be distinguished by X-ray diffraction.[12−28] Thanks to recent technical and methodological developments, the solid-state NMR 'tool-box' now contains a wide and versatile range of one and two-dimensional (2D) experiments that can be adapted to each class of nuclei and materials to allow access to structural pieces of information like the number and multiplicity of crystallographic inequivalents, proximities, or connectivities between neighbors, internuclear distances. These data can then be gradually put together with those extracted from diffraction measurements to assemble a fine structure for a compound, including the description of local disorder or nonperiodic order.

In this contribution, we propose to go beyond the structural description initially given by X-ray powder diffraction[11] and to examine the structural network of aluminum cloverite by means of a set of high-resolution multinuclear (^1H, ^{13}C, ^{15}N, ^{27}Al, ^{31}P, ^{19}F) and multidimensional hetero- and homonuclear solid-state NMR experiments. First, the periodic framework is investigated by 1D ^{31}P and ^{27}Al NMR. 2D $^{31}P-^{31}P$ and $^{27}Al-^{31}P$ correlation NMR experiments are further used to assign the main Al and P resonances. Then, the codirecting agents are characterized by ^{13}C, ^{15}N, and ^1H NMR, and their selective localization in the different pores of the −CLO framework is revealed by 2D $^1H-^1H$ and $^1H-^{31}P$ NMR experiments. Finally, the description of the fluorine subnetwork is done by analysis of $^{19}F-^{31}P$ and $^{19}F-^{27}Al$ 2D NMR correlation spectra. The ensemble of high-resolution NMR results allows a fine description of both the periodic Al/P and the nonperiodic subnetworks, including the selective localization of the organic templates, the position of the F^- ions inside the *D4Rs*, and the nature of the atom or group (OH or F) that form terminal bonds with some of the phosphorus or aluminum atoms. The descriptions of the simple structural rules that obey the F and template subnetworks provide a generalized crystallography, in the sense of A. L. Mackay,[29−31] structure of the aluminum cloverite.

2. EXPERIMENTAL SECTION

2.1. Synthesis. As previously reported in ref 11, DNL-1 was the first aluminophosphate obtained by ionothermal synthesis. The initial mixture of ionic liquid 1-ethyl-3-methylimidazolium bromide ([emim]Br), H_3PO_4, $Al[OCH(CH_3)_2]_3$, HF, and 1,6-hexanediamine (HDA) as a costructure-directing agent was stirred for about one hour at 100 °C. Then the formed gel was heated at 210 °C for two hours in a polytetrafluoroethyl-lined autoclave. LUH-2 was also obtained from H_3PO_4, $Al[OCH(CH_3)_2]_3$, and HF but from an ionic liquid composed of the $[emim]^+$ cation and a mixture of anions, namely bromide and *L*-lactate in a ratio of 7:1. The synthesis mixture was heated for one hour at 160 °C using microwave heating (Explorer-12-Hybrid from CEM).[12] Purity of the samples was checked by powder X-ray diffraction (PXRD). The PXRD diagrams of the two samples (see the SI) are highly similar, indicating identical aluminophosphate network, and are also similar to the PXRD previously reported for aluminum cloverite.[11]

2.2. NMR Spectroscopy. All NMR experiments were performed on an Avance 500 Bruker spectrometer (static magnetic field B_0 = 11.7 T, Larmor frequencies of 500.1, 470.6, 202.5, 125.7, 130.3, and 50.7 MHz for ^1H, ^{19}F, ^{31}P, ^{13}C, ^{27}Al, and ^{15}N, respectively) using either a quadruply tuned 2.5 mm[32] or a 4 mm probe.

The $^1H\rightarrow^{13}C$ cross-polarization magic angle spinning (CPMAS)[33,34] NMR spectrum of $AlPO_4$-(-CLO) was recorded at MAS frequency of 10 kHz. The initial ^1H 90° pulse length was set to 3.1 μs, the contact time to 5 ms. A ^1H RAMped amplitude (RAMP)[35] contact pulse was employed, with a RF field centered on the n = +1 Hartmann−Hahn matching (HHm)[36] condition (i.e., $\nu_{RF}(^1H) = \nu_{RF}(^{13}C) + \nu_{ROT}$) and spanning over $\pm\ \nu_{ROT}$, with $\nu_{RF}(^{13}C)$ = 52 kHz. ^1H 64-step small-phase incremental alternation (SPINAL-64)[37] decoupling (nutation frequency of 70 kHz) decoupling was implemented during the acquisition period. The recycle delay was set to 5 s, and ∼16 000 transients were accumulated. The $^1H\rightarrow^{15}N$ CPMAS NMR spectrum of $AlPO_4$-(-CLO) was recorded at MAS frequency of 12.5 kHz, using a 5 ms contact time, a ^1H RAMP-CP pulse with a RF field centered on the n = +1 HHm and spanning over $\pm\ \nu_{ROT}$. ^1H SPINAL-64 decoupling decoupling was implemented during the acquisition period. The recycle delay was set to 5 s, and ∼60 000 transients were accumulated. The presented ^1H and ^{19}F Hahn-echo MAS (30 kHz) NMR spectra of $AlPO_4$-(-CLO) were recorded using 2.6 μs 90° pulse durations and interpulse delays synchronized with the rotor frequency. ^{19}F Hahn-echo spectra were recorded using various rotor-synchronized interpulse delays. Similar signal intensity decays (thus relaxation times T_2') were observed for all F sites in aluminum cloverite, ensuring that the Hahn-echo sequence does not bias quantitativity of the measurements. The recycle delays were set to 10 s. The ^{31}P single pulse NMR spectrum was taken at MAS 25 kHz using a 160 s recycle delay. ^1H SPINAL-64 decoupling (nutation frequency of 90 kHz) was implemented during the acquisition period. The ^{27}Al single pulse MAS (30 kHz) NMR spectrum was recorded using a 2 μs pulse length. The recycle delay was set to 1 s. The 3Q-MAS experiment was recorded using the three-pulse z-filter[38] sequence, and both dimensions were synchronized with the MAS frequency (28 kHz). Pulse durations to create the triple quantum and the conversion were respectively taken to 3.5 and 1.3 μs with a RF field of 150 kHz. The duration of the selective pulse after the z-filter was 18 μs. 48 t_1 slices with 120 transients each were accumulated. A two-dimensional Fourier transformation followed by a shearing[39] transformation gave a pure absorption 2D spectrum.

The ^{31}P POST-C7[40] NMR spectrum of $AlPO_4$-(-CLO) was taken at MAS 10 kHz, using a 1 ms excitation of the double-quantum coherence. 40 t_1 slices with 336 transients each were accumulated. This 2D DQ-SQ MAS spectrum was converted in a SQ-SQ correlation representation by a shearing transformation.[41,42] The $^{31}P\rightarrow^{27}Al$ heteronuclear correlation (CP-HETCOR) MAS (28 kHz) NMR was recorded using a 2.2 ms contact time; 40 t_1 slices with 1220 transients each were accumulated. For these two experiments, a $^1H\rightarrow^{31}P$ CP block was implemented prior to the DQ excitation or the CP transfer to ^{27}Al to reduce the recycle delay to 5 s (i.e., that of ^1H). The initial ^1H 90° pulse length was set to 2.85 μs, the contact time to 5.5 ms, and a ^1H RAMP contact pulse was employed, with a RF field centered on the n = +1 HHm condition and spanning over $\pm\ \nu_{ROT}$, with $\nu_{RF}(^{31}P)$ = 58 kHz. The conditions used for the CP are similar

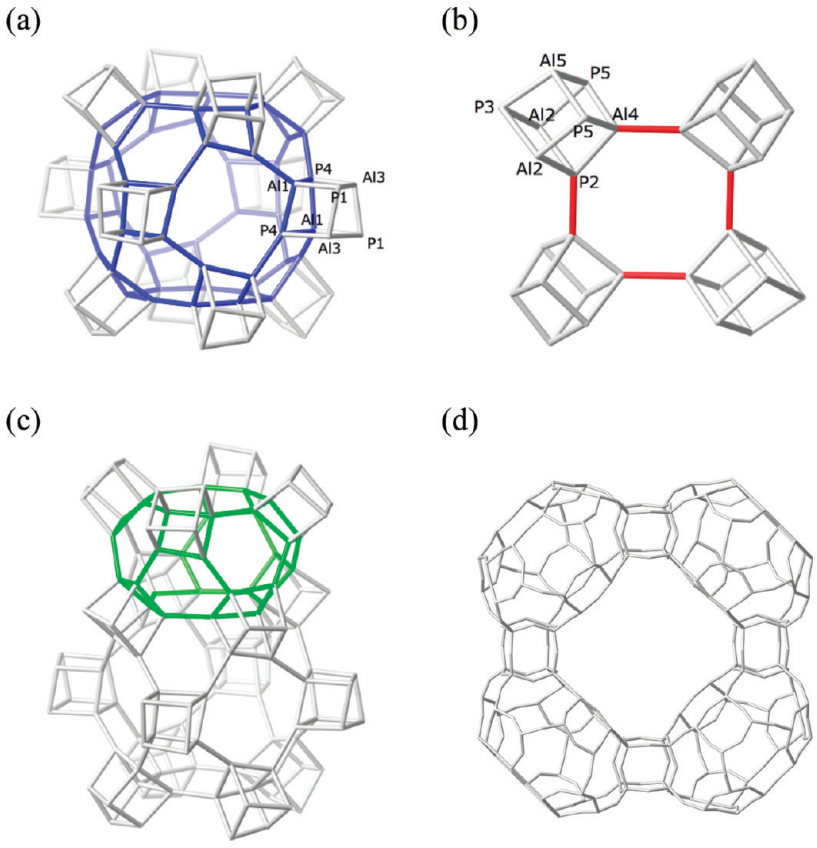

Figure 1. (a) Building unit BU_1 presenting a *LTA*-cavity (in blue), constructed from a 3D assembly of twelve *D4R-1* (in gray), (b) building unit BU_2 constructed from a planar assembly of four *D4R-2* (in gray), and (c) *CLO*-cavity (in green) created at the junction of two building units BU_1 (below) and BU_2 (top). Cationic labeling scheme following the crystallographic sites description is shown. Bridging oxygen atoms have been omitted for the sake of clarity. (d) View of one cavity formed at the intersection of three channels in aluminum cloverite.

than those used to record the 1D CP spectrum. The $^{19}F \rightarrow ^{27}Al$ CP-HETCOR NMR correlation spectrum of CLO-Al was recorded at MAS frequency of 28 kHz, using a low radio frequency (RF) field on the *I*-5/2 ^{27}Al nucleus of ~5 kHz to ensure proper CP transfer[43−45] and a 1.2 ms contact time. 115 t_1 slices with 320 transients each were accumulated. The $^{1}H \rightarrow ^{31}P$ CP-HETCOR MAS (28 kHz) NMR spectrum was recorded using a 5.5 ms contact time. 260 t_1 slices with 48 transients each were accumulated. The $^{19}F \rightarrow ^{31}P$ CP-HETCOR MAS (28 kHz) NMR spectrum of $AlPO_4$-(-CLO) was recorded using a 5 ms contact time. 115 t_1 slices with 256 transients each were accumulated. The 2D ^{1}H DQ-SQ MAS (25 kHz) NMR spectrum was acquired using the back-to-back (BABA)[46] recoupling sequence with a delay of 240 μs for the excitation and reconversion of the double-quantum coherence. 80 t_1 slices with 64 transients each were accumulated. In all 2D NMR experiments, phase sensitive detection in the indirect dimension was obtained using the States[47] method.

The ^{13}C, ^{1}H, ^{15}N, ^{19}F, ^{31}P, and ^{27}Al chemical shifts were referenced to the carbon and proton signal in TMS, nitrogen signal from ^{15}N-enriched glycine (−347.5 ppm from nitromethane),[48] $CFCl_3$, H_3PO_4 85%, and a 1 M solution of $Al(NO_3)_3$, respectively. The spectra were reconstructed using the Dmfit[49] software.

3. RESULTS AND DISCUSSIONS

The aluminum cloverite, $AlPO_4$-(-CLO), crystallizes in the cubic crystal system (space group n° 226: $Fm\bar{3}c$) with a unit cell parameter of 51.363 Å.[11] Its structure is build up from two types of *D4R*s units composed from strict alternation of corner-sharing AlO_4 and PO_4 tetrahedra. The first building unit (BU_1) is a rather spherical α-cavity (*LTA* composite building unit) resulting from the 3D assembling of twelve *D4R-1* (Figure 1a). The *D4R-1* cages contain 2 inequivalent P atoms (P1 and P4) and two 4-fold coordinated inequivalent Al atoms (Al1 and Al3). A planar assembly of four *D4R-2* forms the second building unit BU_2 (Figure 1b). The *D4R-2* cages contain 3 inequivalent P atoms (P5 of multiplicity 1 and P2 and P3 of multiplicity 1/2) and 3 inequivalent Al atoms (Al2 of multiplicity 1, Al4 and Al5 of multiplicity 1/2). The connection of two building units BU_1 and BU_2, alternating in the three-dimensional space, forms the *CLO*-cavity (Figure 1c) that takes its name from the topology of the material. As in the gallium cloverite-type structure, the framework of the aluminum cloverite-type structure shows an intersecting 3D channel system with 20-ring windows, as shown in Figure 1d. At the intersection of the channels, four terminal hydroxyl groups (Al5-OH or P3-OH) extend from the *D4R-2* to give the window a cloverleaf shape in which half of the *D4R*s are not fully connected. The template molecules, not represented, occupy the space available either in the *LTA*-pores or at the intersections of the channels (Figure 2).

3.1. Aluminophosphate Network. In this section, we present the characterization of the periodic aluminophosphate network of $AlPO_4$-(-CLO) by 1D ^{31}P and ^{27}Al NMR as well as 2D $^{31}P-^{31}P$ and $^{31}P-^{27}Al$ correlation experiments. The inorganic subnetwork is common to both DNL-1 and LUH-2 samples, and so are their ^{27}Al and ^{31}P NMR spectra. Therefore, when not

dx.doi.org/10.1021/cm2021033 |*Chem. Mater.* 2011, 23, 4799–4809

specified, the NMR spectra presented in the following section are the signatures of both DNL-1 and LUH-2.

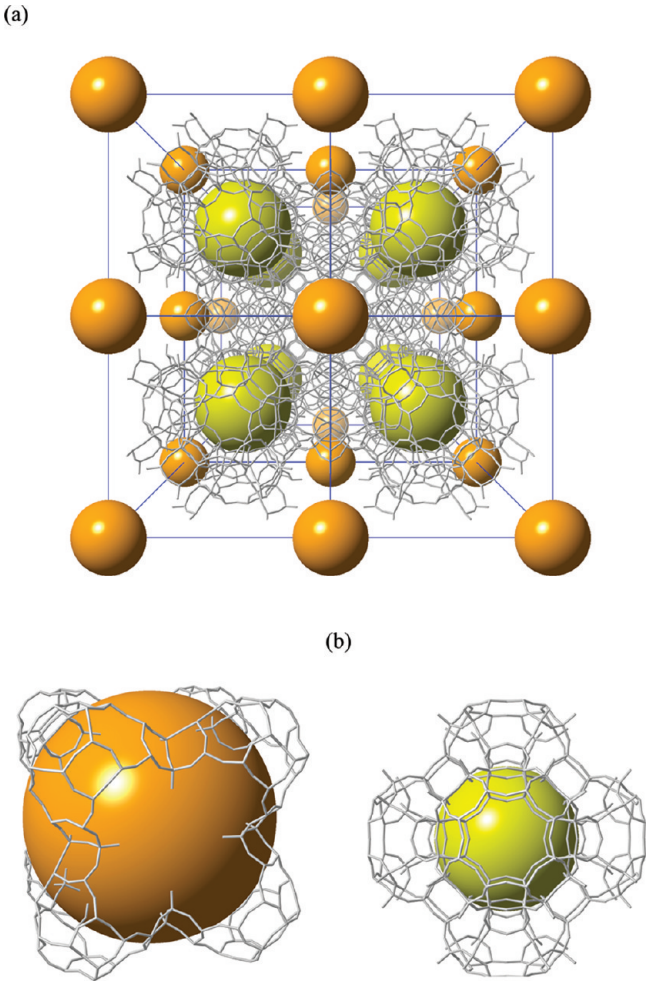

Figure 2. (a) Perspective view of the structure of aluminum cloverite. The gray sticks represent the Al/P framework. The yellow and dark yellow balls are placed so that they fill the cavities (yellow balls) and channels (dark orange balls) of the framework. For the sake of clarity, the dark orange balls have been sized down. (b) Representations of the filled channel intersections (left) and *LTA*-pores (right).

^{27}Al NMR. The ^{27}Al MAS NMR spectrum of the aluminum cloverite is displayed in Figure 3a and shows three main signals centered on 38.2 ppm, 22.9 ppm, and −7.1 ppm (Table 1), characteristic of aluminum atoms in 4- (Al^{IV}), 5- (Al^{V}), and 6- (Al^{VI}) fold coordination.[50] The ^{27}Al resonances are broad and show a tail on their right part characteristic of distributed environments around the Al atoms. The positions of the ^{27}Al lines are slightly different from what was earlier reported on lower static magnetic field (9.4 T),[11] which can be explained by a more efficient reduction of the effects of the second order of the quadrupolar interaction (^{27}Al nuclear spin $I = 5/2$) at higher magnetic field (11.7 T in our study). The higher magnetic field we employed also increases the resolution of the Al signatures, and at least two contributions for the Al^{IV} can be distinguished. According to the structural data, five different Al^{IV} sites are expected in DNL-1, but only two of them are resolved on the 1D NMR spectrum and a 2D ^{27}Al 3Q-MAS NMR spectrum (Figure 3b) did not improve the spectral resolution (reconstruction of the spectrum is provided in the SI). Since all aluminum atoms are in 4-fold coordination in the *CLO*-type structural model, the presence of higher coordination numbers for the Al atoms was assumed to be caused by the interaction of the aluminum with fluorine and water molecules.[51,52] To confirm this hypothesis, the DNL-1 sample was dried overnight at 100 °C, and a similar ^{27}Al 1D MAS NMR spectrum was taken (Figure 3a ii). It should be mentioned that the PXRD pattern of the dried sample is identical to that of the initial one, including similar diffraction peak line width (see the SI), indicating that the drying has affected neither the structural network nor the crystallinity of the sample. This is also supported by the ^{27}Al NMR lineshapes which remained essentially similar upon drying (see the SI). The striking point of the ^{27}Al NMR spectrum of the dried sample is the strong decrease of the Al^{VI} contribution associated with an increase of the Al^{IV} contribution and almost no change in the intensity of that of the Al^{V} aluminum atoms. This indicates that in the sample stored in air, the first coordination spheres of some of the aluminum atoms are indeed completed by two oxygen atoms from absorbed water molecules. This is supported by the ^{1}H NMR spectra (see the SI) recorded on the sample before and after drying, for which the broad ^{1}H resonance centered on 5 ppm, characteristic of water molecules, has disappeared after drying. To the contrary, the extra-ligand that results in the formation of a 5-fold coordinated aluminum

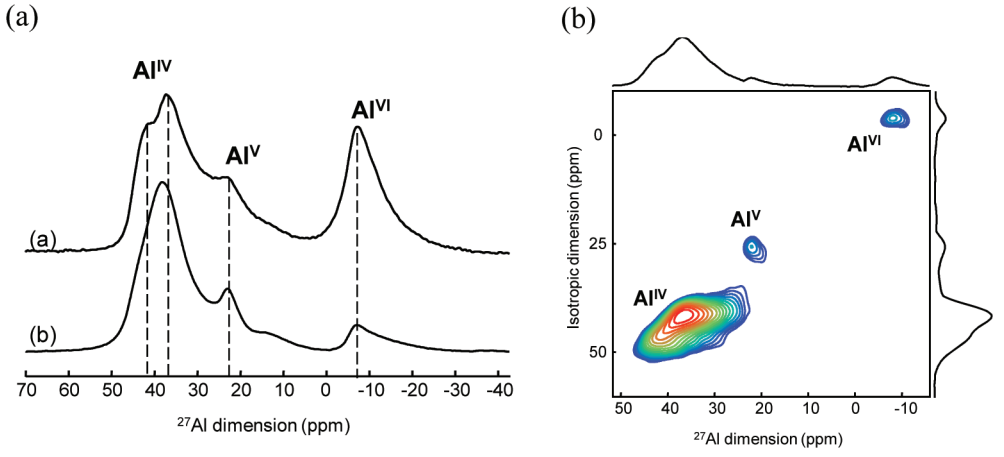

Figure 3. (a) ^{27}Al MAS NMR spectra of the aluminophosphate DNL-1 before (i) and after (ii) overnight drying at 100 °C. Lines are assigned to the aluminum atoms in 4-, 5-, and 6-fold coordination. The dashed lines are guides for the eye. (b) ^{27}Al 3Q-MAS NMR spectrum of the dried DNL-1 sample.

dx.doi.org/10.1021/cm2021033 |*Chem. Mater.* 2011, 23, 4799–4809

Table 1. Line Number, Relative Intensity (%), Isotropic Chemical Shift (ppm) (Position of the Center for the ^{27}Al Resonances), and Line Assignment Deduced from the ^{31}P, ^{27}Al, and ^{19}F MAS NMR Data of Aluminum Cloverite

line	δ_{iso} (±0.1)	intensity (±1)	assignment
		^{31}P	
1	−7.1	8	P3-OH
2	−18.7	48	P1 + P4
3	−23.8	23	P5
4	−28.9	21	P2 + P3
		^{27}Al	
1	38.2	74	Al^{IV}
2	22.9	16	Al^{V}
3	−7.1	10	Al^{VI}
		^{19}F	
1	−95.4	58	F^- in *D4R*
2	−126.4	28	F−P terminal
3	−144.8	14	F−Al terminal

atom is probably not an oxygen atom from a water molecule, since it is not affected by the overnight drying, but most likely a fluorine atom. This is confirmed by the ^{27}Al MAS NMR spectrum taken a couple of days after that the dried sample was stored under air (see the SI), which shows the growth of the Al^{VI} component but almost no change in the Al^{V} atoms. The Al^{VI} component could not be completely removed by a simple overnight drying and the remaining proportion can be estimated by integration of the resonance to ∼10% of the total amount of aluminum atoms. The Al^{V}/Al^{IV} relative ratio, also estimated by integration of the two parts of the spectrum, is around 1:3.

Because of the changes upon dehydration observed on the ^{27}Al NMR spectra, all the NMR experiments presented in the following sections were recorded on the aluminum cloverite sample previously dried overnight at 100 °C.

^{31}P NMR. The ^{31}P MAS NMR spectrum of the $AlPO_4$-(-CLO) (Figure 4) exhibits four resonances located at isotropic chemical shifts (δ_{iso}) of −7.1 ppm, −18.7 ppm, −23.8 ppm, and −28.9 ppm (Table 1). Again the higher magnetic field employed in our study increases the resolution of the ^{31}P signals compared to the earlier reported spectra[11] and allows the resolution of two additional lines. The ^{31}P resonances are fairly broad (0.8−1 kHz at half width) and cannot be narrowed by ^{1}H decoupling, indicating that the ^{31}P line width is mostly due, as was also observed on the ^{27}Al MAS NMR data in the previous section, to chemical shift distribution, i.e. distribution of environments around the P atoms, rather than to dipolar couplings with the neighboring protons. As mentioned above, in aluminum cloverite, the phosphorus atoms occupy five inequivalent positions of relative multiplicity 1:1:1:1/2:1/2 for P1, P4, P5, P2, and P3, respectively (Figure 1), but only four of them can be distinguished on the ^{31}P MAS NMR spectrum (Figure 4). The ^{31}P relative line intensities were estimated by reconstruction of the spectrum line shape to 8%, 48%, 23%, and 21%, for lines 1, 2, 3, and 4, respectively. The ^{31}P line 1 has a high chemical shift (−7.1 ppm) characteristic of phosphorus atom in a P−OH group and is therefore assigned to terminal P3-OH atoms. The relative intensity of line 1 is slightly lower than what was expected (12.5% for 1 P atom on a site of 1/2 multiplicity), which could indicate that some of the P3 atoms have no OH group in their vicinity. Line 4, of second lowest intensity, is therefore assigned to P2 and possibly the P3 atoms with no terminal OH bond. Lines 3 of multiplicity 23% (1 P site) and line 2 multiplicity 48% (2 P sites) correspond to the P atoms of highest multiplicity P1, P4, and P5 but cannot be assigned more precisely. To complete the ^{31}P spectrum assignment, ^{31}P−^{31}P 2D double-quantum single-quantum (DQ-SQ) MAS NMR correlation experiment, generating using the ^{31}P−^{31}P dipolar interaction, was used to probe the phosphorus−phosphorus spatial proximities. To ease reading of the spectrum, the DQ dimension has been sheared, as mentioned in the Experimental Section, into a SQ dimension. In such a spectrum, off-diagonal correlation peaks appear at the isotropic chemical shift of neighboring P atoms with distinct chemical shift values, while dipolar-coupled P atoms with identical chemical shifts will generate a diagonal peak. Moreover, the DQ recoupling scheme is based on dipolar interaction, and the intensity of the cross-peaks therefore decreases with increasing P−P internuclear distance. The ^{31}P 2D DQ-SQ NMR spectrum of the aluminum cloverite (Figure 5) shows that the cross-correlation peak with the strongest intensity for P3 (line 1) is with line 3, of double intensity, which is consequently assigned the P atom of double multiplicity located in the same *D4R-2* unit near P3, i.e. P5. Line 2, which corresponds to two P atoms of double intensity, contains therefore the signatures of P1 and P4. These two P atoms belong to the *D4R-1* unit, as shown by the diagonal peak of strong intensity for line 2. Line 3, assigned to P5, exhibits correlation peaks with P atoms belonging to *D4R-1* and *D4R-2*, indicating that it acts as linker between the two types of units (Figure 1). This 2D ^{31}P NMR correlation spectrum confirms the main topological features of the *CLO*-type network and allows a full assignment of the ^{31}P resonances.

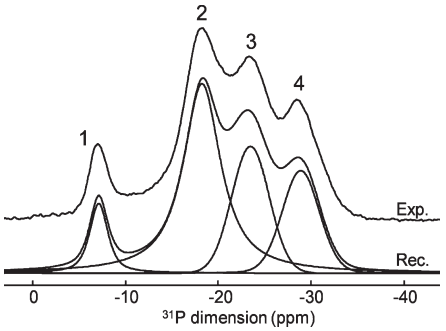

Figure 4. Experimental and reconstructed ^{31}P MAS NMR spectra of the aluminum cloverite on which lines are labeled.

^{31}P−^{27}Al 2D CP-MAS NMR. The ^{31}P→^{27}Al 2D CP-HETCOR NMR correlation spectrum of aluminum cloverite (Figure 6) shows improved resolution in the ^{27}Al dimension as compared to the ^{27}Al 1D or 3Q-MAS NMR spectra (Figure 3), and four distinct aluminum resonances can be distinguished: one 5-fold Al and three 4-fold Al (out of the five expected from the structural model) atoms. The ^{31}P→^{27}Al 2D CP-HETCOR NMR correlation spectrum exhibits cross-peaks between the ^{31}P line assigned to P3 with the Al^{IV} resonance of highest chemical shift. As expected, this Al site is also correlated to the line assigned to P2, while the line corresponding to P5 has a cross-peak with the Al resonance of second highest position. This corroborates the assignments of these three ^{31}P lines, deduced from the 2D ^{31}P NMR spectrum, to phosphorus atoms belonging to the same *D4R* unit (Figure 1). The lines corresponding to P1 and P4 are

dx.doi.org/10.1021/cm2021033 |*Chem. Mater.* 2011, 23, 4799–4809

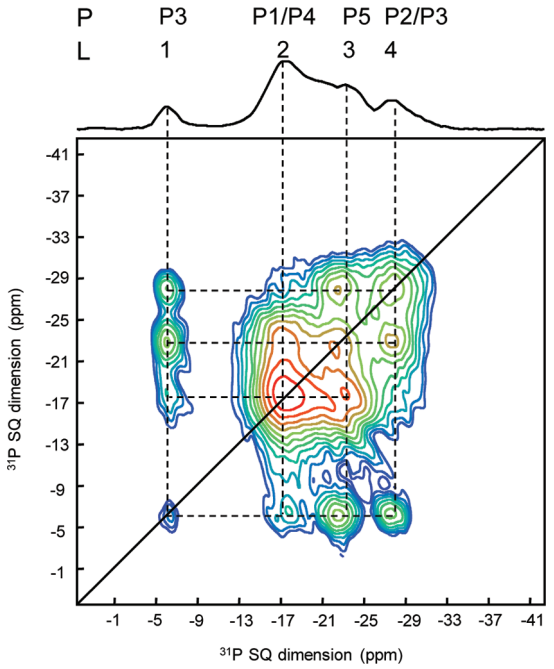

Figure 5. ^{31}P POST-C7 NMR spectrum of aluminum cloverite. The top spectrum, on which lines (L) are labeled and assigned to the corresponding phosphorus atoms (P), is the full projection on the horizontal dimension. Dashed lines indicate P−P proximities.

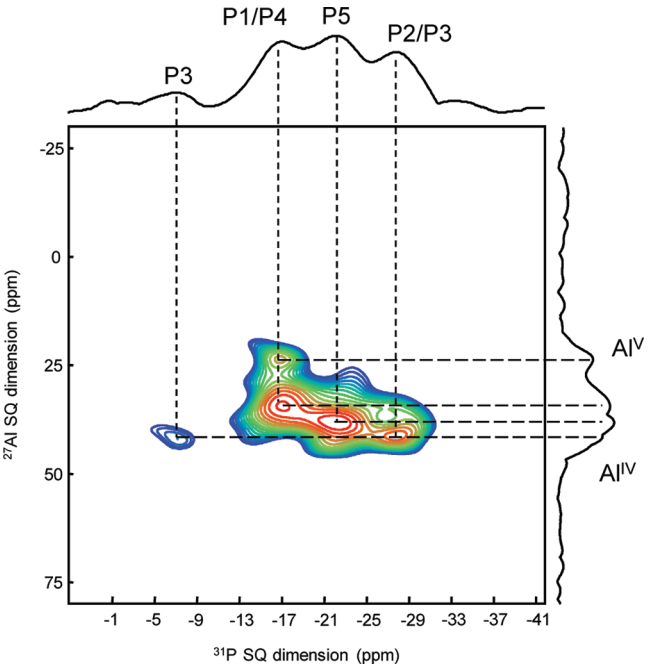

Figure 6. ^{31}P→^{27}Al MAS CP-HETCOR NMR spectrum of aluminum cloverite. Top and right spectra, on which lines are labeled, are the full projection on the ^{31}P and ^{27}Al dimension, respectively. Dashed lines indicate P−Al proximities.

close to the same Al^{IV} site, which has the lowest chemical shift. Again, this validates the assignment of the ^{31}P lines to phosphorus atoms belonging to the same *D4R*. It should be pointed out that the local environments of the P and Al atoms within the *D4R-1* unit are probably much more similar than between the P and Al atoms in the *D4R-2* since neither the P nor the Al sites can be distinguished on the ^{31}P and ^{27}Al NMR spectra. One can notice the absence of any cross-correlation peaks between the P atoms and the 6-fold coordinated Al atoms. Two independent reasons could be invoked: i) the sensitivity of the CP-HETCOR NMR experiment to the ^{27}Al offset carrier frequency might have reduced the recoupling efficiency between the P and Al^{VI} and ii) the Al^{VI} is coordinated to four P but also to two O atoms from water molecules. The water molecules are located in the interrupted parts of the network and are very likely mobile. This mobility can strongly reduce the ^{27}Al relaxation times, leading to a decrease of the CP efficiency. Finally, the ^{31}P→^{27}Al 2D CP-HETCOR NMR correlation spectrum of $AlPO_4$-(-CLO) also contains a correlation peak between the 5-fold coordinated aluminum atoms and P1 and P4. Although low intensity correlation between Al^{V} and the other P atoms cannot be excluded, the spectrum clearly indicates that the Al^{V} mostly belong to the *D4R-1*.

The assignments of the ^{27}Al and ^{31}P resonances to the various sites of aluminum cloverite are gathered in Table 1.

3.2. Templating Agents. Contrary to the gallium cloverite, for which the topology has been obtained using a single templating amine (quinuclidine), two amines, whose structures are depicted in Figure 7a, have been used as co-SDAs to build up the topology of DNL-1:[11] ethyl-methyl-imidazolium $C_6H_{11}N_2$ ($[emim]^+$) cations and diprotonated 1,6-hexane-diamine $C_6H_{18}N_2$ (HDA). Only the characterization of the DNL-1 sample is presented in this section, because it contains two distinct amines. The characterization of the amines and their localization in the structure is essential to better understand the role and potential selectivity of these templates.

^{13}C NMR. The ^{1}H→^{13}C CP-MAS NMR spectrum of DNL-1 (Figure 7b) shows two types of ^{13}C resonances (Table 2): broad signals from the carbon atoms of the HDA and a set of much narrower peaks that correspond to the carbon atoms of the $[emim]^+$ cations.[11] The ^{13}C resonance from the HDA located at 40.2 ppm (relative intensity of 1) correspond to the carbon atoms in α position from the amino groups, while that located at 26.6 ppm (relative intensity of 2) corresponds to the carbon atoms in β and γ positions.[11] Despite the use of ^{1}H decoupling, the ^{13}C resonances of the HDA remain unusually broad (∼600 Hz), indicating a static distribution of the positions or orientations of the HDA molecules in the pores of the aluminophosphate. Five sets of much narrower peaks (∼100 Hz) can be distinguished, which correspond to the carbon atoms from the $[emim]^+$ cations. Each of these main peaks actually contain two contributions, indicating that, contrary to the randomly located HDA molecules, the $[emim]^+$ occupy two inequivalent and well-defined crystallographic positions in the pores of DNL-1. One can notice a broadening of the base of the ^{13}C peaks at higher chemical shift. These peaks correspond to the three quaternary carbon atoms, which are surrounded by one or two nitrogen atoms, and the broadening could therefore arise from an interaction with the quadrupolar spin-1 ^{14}N nuclei.

^{15}N NMR. The ^{1}H→^{15}N CP-MAS NMR spectrum of DNL-1 recorded under ^{1}H decoupling (Figure 7c) also shows two sets of ^{15}N resonances with different apparent line width (Table 2). One broad (line width ∼270 Hz) signal is located at −356.7 ppm and corresponds to the sp^3 nitrogen atoms of the HDA molecules. Two narrower (line width ∼90 Hz) signals are located at −202.4

dx.doi.org/10.1021/cm2021033 |*Chem. Mater.* 2011, 23, 4799–4809

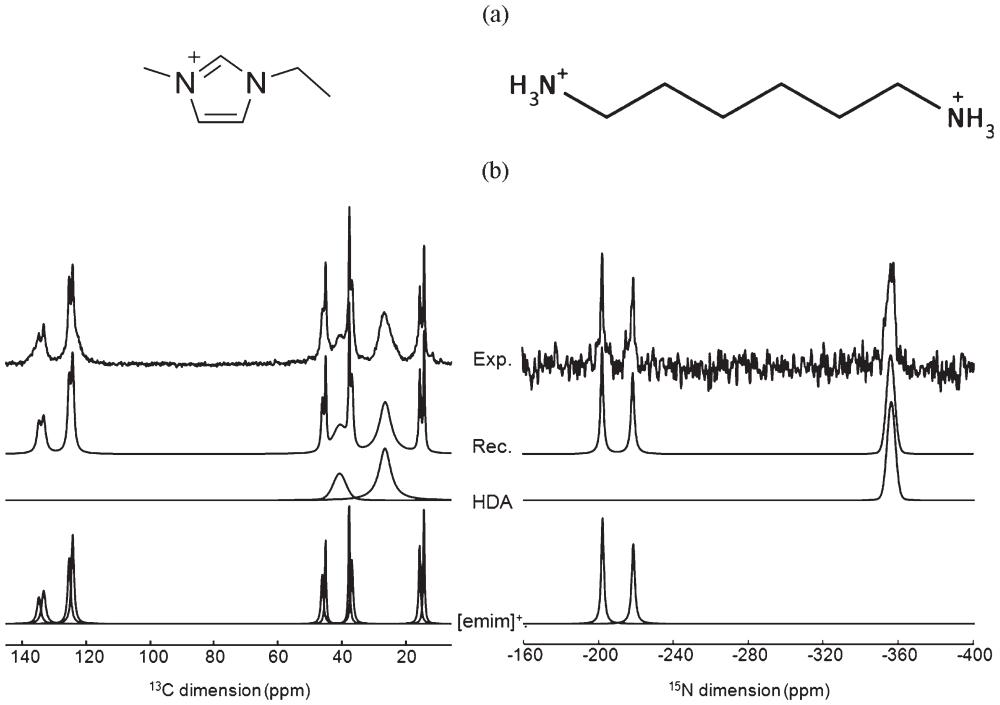

Figure 7. (a) Structures of the two co-SDAs used to build up the DNL-1 framework: $[emim]^+$ (left) and HDA (right). (b) Experimental and reconstructed $^1H \rightarrow ^{13}C$ (left) and $^1H \rightarrow ^{15}N$ (right) CPMAS NMR spectra of DNL-1. The individual contributions from the two co-SDAs are shown.

Table 2. Isotropic Chemical Shift (ppm) and Line Assignment Deduced from the ^{13}C and ^{15}N CPMAS NMR Data of DNL-1

δ_{iso} (±0.1)	assignment
^{13}C	
40.2	HDA
26.6	
134.4	$[emim]^+$
133.9	
124.9	
123.8	
45.6	
44.6	
37.2	
36.3	
15.1	
13.7	
^{15}N	
−356.4	HDA
−202.4	$[emim]^+$
−218.7	

and −218.7 ppm and correspond to the two sp^2 nitrogen atoms of the $[emim]^+$ cations. Contrary to the ^{13}C NMR spectrum, no splitting of the ^{15}N resonance of the $[emim]^+$ is observed, which could be due to the lower chemical shift sensitivity of the ^{15}N nucleus compare to ^{13}C one. The larger line width of the ^{15}N resonance from the HDA molecule confirms the distribution of positions or orientations of the HDAs.

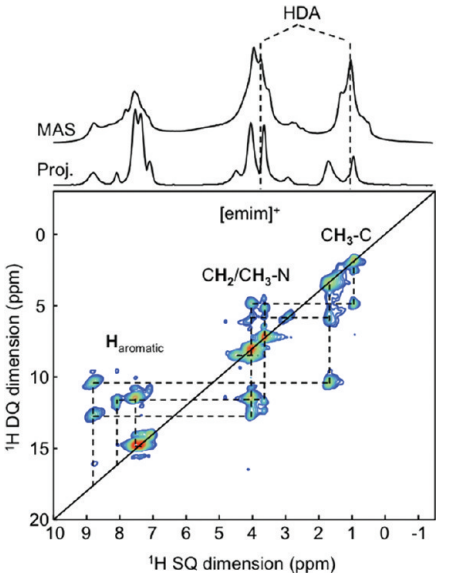

Figure 8. ^1H 2D DQ-SQ NMR correlation spectrum of the aluminophosphate DNL-1. Dashed lines indicate H−H proximities. The top spectrum (Proj.) is the full projection on the ^1H SQ dimension, on which the components of the HDA are missing. Above is depicted the ^1H MAS NMR spectrum.

The ^{13}C and ^{15}N NMR data indicate that the $[emim]^+$ cations occupy two distinct and well-defined crystallographic positions. To the contrary, the HDA molecules are randomly oriented in the pores, and this nonperiodic feature is very likely at the origin of the distribution of chemical shifts observed on the ^{27}Al and ^{31}P NMR spectra of DNL-1.

dx.doi.org/10.1021/cm2021033 |Chem. Mater. 2011, 23, 4799–4809

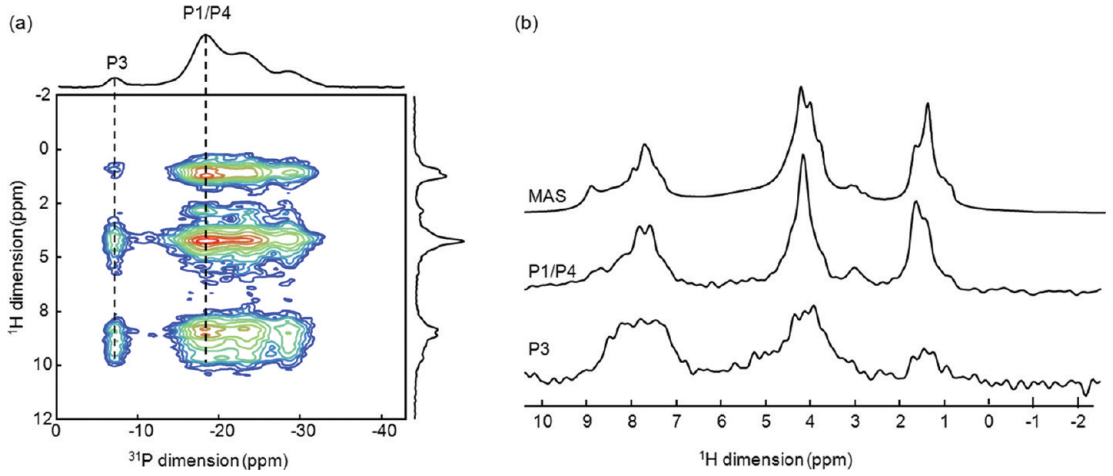

Figure 9. (a) 2D ^{1}H→^{31}P CP-HETCOR NMR spectrum of the aluminophosphate DNL-1. The top spectrum, on which lines are labeled, is the full projection on the ^{31}P dimension. Dashed lines indicate the positions of the slices shown in (b). (b) ^{1}H MAS and vertical slices taken from the 2D ^{1}H→^{31}P CP-HETCOR NMR spectrum at the positions of P3 and P1/P4.

^{1}H−^{1}H and ^{1}H−^{31}P 2D NMR. To determine more precisely the localization of the two different co-SDAs in the various pores of the CLO-type framework (*CLO* or *LTA* cavities), spatial proximities between the protons of the co-SDAs and between protons and the phosphorus atoms from the framework have been probed by 2D ^{1}H−^{1}H and ^{1}H−^{31}P NMR experiments, respectively. The ^{1}H MAS NMR spectrum of DNL-1 (Figure 8, top spectrum) can be divided in three main parts: the signals in the 7−9.5 ppm range are characteristic of protons in an aromatic ring, the signals in the 2−6 ppm range corresponds to protons from CH_2 and CH_3 groups next to N atoms and to the protons from the NH_3 group of the [emim]$^+$, and the signals in the 0.5−2.5 ppm range correspond to proton from CH_3 and CH_2 groups next to C atoms. The ^{1}H DQ-SQ NMR spectrum of DNL-1 (Figure 8) contains the signature of the neighboring protons of the amines and to be read as the ^{31}P 2D NMR spectrum: two protons close in space to each other (i.e., H−H distance below 4 Å) generate a peak on the diagonal if they have the same chemical shift or a pair of off-diagonal cross-peaks if they have different chemical shifts. The absence of peaks between two lines indicates that the corresponding protons are far from each other. A comparison between the ^{1}H MAS NMR spectrum and the full projection of the 2D spectrum along the direct dimension shows that two components from the nonaromatic regions, located at 4.0 and 1.5 ppm, are missing on the 2D map. These peaks are therefore assigned to the protons from the NH_3 and CH_2 groups of the HDA molecules, respectively. The ^{1}H 2D NMR experiment indeed makes use of the ^{1}H−^{1}H homonuclear dipolar interaction to edit the proximities between the protons. Any motion of the protons faster than the dipolar time scale will average out this interaction, and the DQ-SQ will filter out the signals of the corresponding protons.[53−55] Consequently, the absence of signal of the HDA on the 2D NMR spectrum could be explained by rapid motions of the NH_3 and possibly the CH_2 groups around the N−C and C−C single bonds that average out the dipolar interaction. On the 2D NMR spectrum mostly remain the signatures of the [emim]$^+$. More ^{1}H resonances are observed than what was expected from the structure (six inequivalent proton sites), which confirms the two inequivalent positions for the [emim]$^+$.

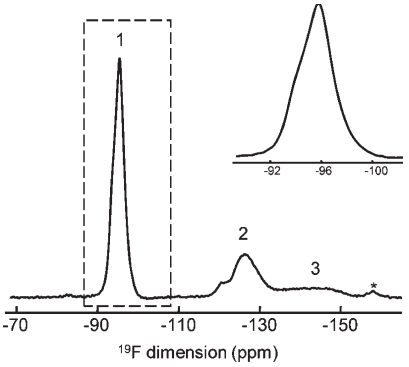

Figure 10. ^{19}F MAS NMR spectrum of the aluminophosphate DNL-1, on which lines are labeled. Stars indicate the position of spinning sidebands. An expansion of the high chemical shift region is given in inset.

The ^{1}H→^{31}P CP-HETCOR NMR spectrum of DNL-1 (Figure 9a) shows the spatial proximities between the P atoms from the framework and the protons from the templates. To discriminate the two possible pores in which the templates can sit, two slices at the position of P3-OH (only present at the intersection of the channels) from the *D4R-2* and at the position of P1 and P4 (present in both the spherical *LTA*-cavities and at the intersection of the channels) from the *D4R-1* have been extracted from the 2D spectrum and compared to the MAS NMR spectrum (Figure 9b). The slice at P1 and P4 is very similar to the MAS spectrum, which indicates that these P atoms have both an [emim]$^+$ and HDA molecules in their vicinity. To the contrary, on the slice taken at P3 (Figure 9b), mostly remain the signals of the protons from the aromatic region (7−9.5 ppm range), i.e. the P3 atoms are close to the [emim]$^+$ cations. This indicates that the space at the intersection of the channels is free from HDA molecules, in other words the HDA molecules yield spherical *LTA*-pores rather than channels. Finally, it should be mentioned that the CLO-type framework has been obtained with different templates, quinuclidine for CLO-Ga or co-SDAs HDA and [emim]$^+$ for the DNL-1. Therefore, the selectivity of the CLO-type framework to the templating agent(s) may not be so critical.

dx.doi.org/10.1021/cm2021033 |*Chem. Mater.* 2011, 23, 4799–4809

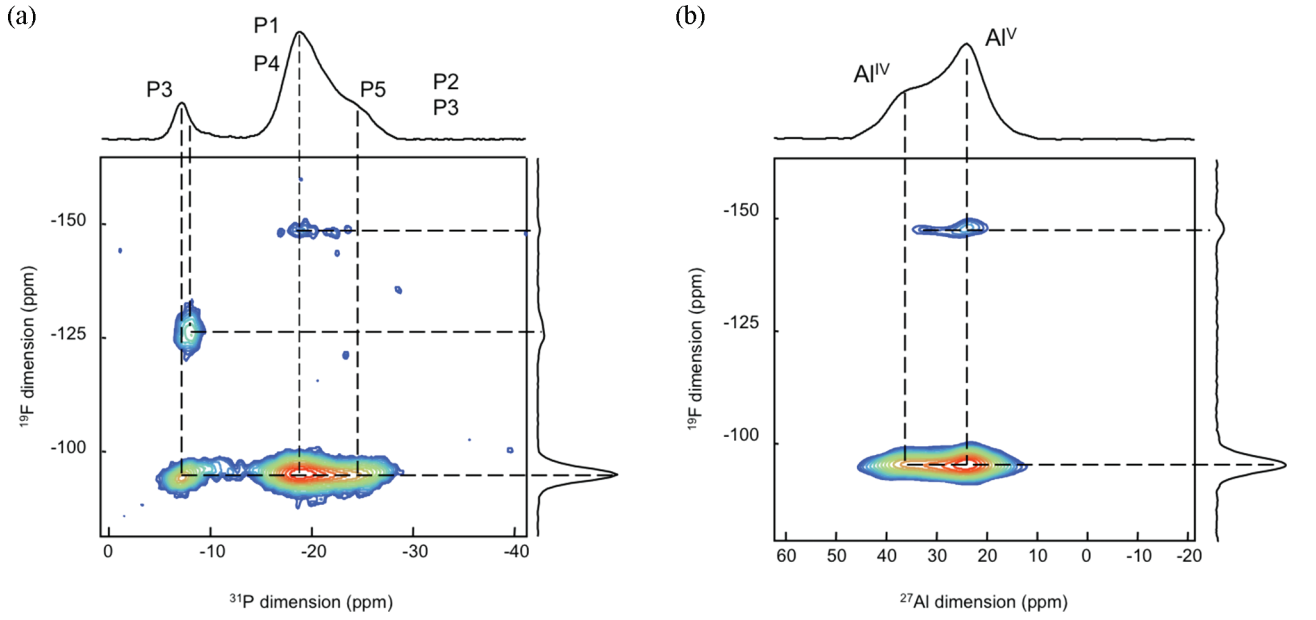

Figure 11. ^{9}F→^{31}P (a) and ^{19}F→^{27}Al (b) CP-MAS NMR spectra of the aluminophosphate DNL-1. Top spectra, on which lines are labeled, are the full projection on the ^{31}P and ^{27}Al dimensions. Right spectra are the full projections on the ^{19}F dimension. Dashed lines indicate ^{31}P/^{27}Al−^{19}F proximities.

3.3. Fluorine Subnetwork. *^{19}F NMR.* In the ^{19}F MAS NMR spectrum (Figure 10) of DNL-1, the main signals are observed at −95.4, −126.4, and −144.8 ppm. As previously seen in various aluminophosphate types (e.g., *LTA*- and *AST*-type),[47,56] the resonance at −95.4 ppm corresponds to F^- ions trapped in *D4R* units of the structure (Figure 12a). An expansion of this line shows that it actually contains two resonances (Figure 10). The two kinds of trapped F^- ions can be related to different interactions between the F and its surrounding atoms in the *D4R-1* or in the *D4R-2* cages. The other peaks, broader and of lower intensity, were assigned to the presence of fluorine terminal atoms as Al−F or P−F groups.[57] It should be mentioned that ^{1}H decoupling has no apparent effect on the ^{19}F NMR line width (corresponding spectrum not shown), indicating that the line widths are also mostly heterogeneous and due to chemical shift distributions, similarly to what was observed in the previous sections for the ^{31}P and ^{27}Al nuclei. To further investigate the location the F atoms in the network, 2D correlation NMR experiments were carried out and are presented in the following.

^{19}F−^{27}Al and ^{19}F−^{31}P 2D NMR. Such 2D NMR experiments, based on the ^{19}F-X (X = ^{31}P or ^{27}Al) heteronuclear dipolar interaction, allow probing the spatial proximities between the fluorine and the aluminum and phosphorus atoms. The ^{19}F→^{31}P 2D CP-HETCOR NMR spectrum of DNL-1 is displayed in Figure 11a. It shows a cross peak of strong intensity between P1 and P4 and the F line located at −95.2 ppm, indicating the presence of F- ions trapped in the *D4R-1* units (Figure 12c). There are also cross-peaks between P3 and P5 from the *D4R-2* unit with F^- ions at −95.2 ppm. But the intensities are much lower than the P−F cross-correlation peak of the *D4R-1* and could not be detected for P2. This very likely indicates that there are less *D4R-2* units occupied by a F^- ion (Figure 12d). Moreover, the ion very likely does not stand in the middle of the cubic cage but rather closer to one corner of the cubic *D4R*. Moreover, one can notice a cross-correlation peak between P3 and the F atom located at −126.4 ppm. This ^{19}F resonance, which corresponds to about 25% of the total amount of fluorine in the sample, is therefore assigned to a F atom not trapped in a *D4R* (different ^{19}F chemical shift and much broader line) and bonded to a terminal P3 atom. The ^{31}P chemical shift of the phosphorus atoms from this P3−F group is slightly different from the chemical shift of the P atom in a P3-OH group and has no correlation with the F resonance from the trapped F^- ions. This clearly indicated that the *D4R-2* units can only be occupied by a F^- ion if the terminal P3 is covalently bonded to an OH group and not to a F atom. In other words, a P−F terminal group prevents the trapping of F^- ion in the corresponding *D4R* cage (Figure 12).

The ^{19}F→^{27}Al 2D CP-HETCOR correlation NMR spectrum of DNL-1 (Figure 11b) shows that the F^- ions are mostly correlated to the 5-fold coordinated Al atoms. This confirms that the F^- ions do not stand in the middle of the *D4R* unit but are closer to a corner of the cube and enter in the coordination shell of the aluminum atoms (Figure 12), as was previously observed for example in oxyfluorinated gallium phosphate ULM-18.[58] In such a situation, the distance of the F with the Al^{IV} sitting at the opposite corner is longer, thus the lower intensity of the corresponding cross-correlation peak. The ^{19}F→^{27}Al 2D CP-HETCOR correlation NMR spectrum contains an additional peak between an Al^{V} and a F atom outside the *D4R* (−144.8 ppm), indicating the presence of Al−F terminal bonds. This F site also correlates with the P1 and P4 atoms (Figure 11a), and therefore this interruption mostly concerns some the *D4R-1*. One can notice the absence of the Al^{VI} resonance, very likely because the increased coordination is caused by water molecules rather than by F atoms. The final assignments of the ^{27}Al, ^{31}P, and ^{19}F NMR resonances to the various sites of aluminum cloverite are gathered in Table 1, and a summary of the possible situations extracted from analysis of the NMR data is presented in Figure 12.

Although some structural details, for which we have no NMR evidence, still remain unknown, like whether the water molecules coordinate the aluminum atoms from both the *D4R-1* and *D4R-1* or only one of them selectively (i.e., what is the role of the

dx.doi.org/10.1021/cm2021033 |*Chem. Mater.* 2011, 23, 4799–4809

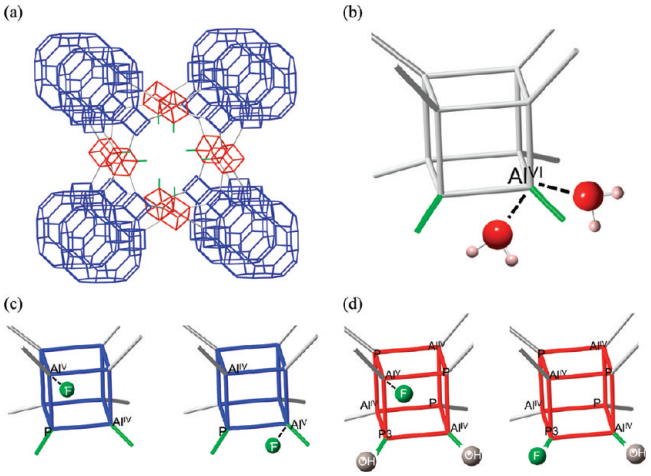

Figure 12. (a) Perspective view of the cloverleaf-shaped intersection of the channels in aluminum cloverite, build-up from *D4R-1* (blue) and *D4R-2* (red) units. In green are the bonds to the terminal F/OH atoms (Al−F/OH and P−F/OH), exclusively found in the channels. (b) Schematic representation of the two water molecules that generate the 6-fold coordinated Al atoms. Schematize representations of possible situations for the (c) *D4R-1* and (d) *D4R-1* cages. For the sake of clarity, only the bonds to the neighboring *D4Rs* are represented (gray sticks). (c) *D4R-1* cage: (left) in which a F^- ion is trapped. The F^- ion does not sit at the center of the *D4R* cage but is closer to one aluminum atom, which becomes 5-fold coordinated (Al^V); (right) in which a terminal F atom is bonded (dashed line) to one Al atom (which become 5-fold coordinated) from outside the cage. This extra F atom is also in the proximity of one P atom. (d) *D4R-2* cage: (left) in which a F^- ion is trapped. The terminal atom is then an OH group; (right) in which one Al atom is bonded to a terminal F atom, preventing the insertion of a trapped F^- ion in the cage.

terminal F atom in this aspect), or whether there is an OH group inside the *D4R-2* when the terminal atom is a F, this thorough set of NMR experiments has allowed going beyond the structural description of the aluminum cloverite sample initially provided by powder diffraction, by evidencing several distinct possible locations for the F atoms, OH groups, and water molecules as well as the templating agents in the framework of the aluminum cloverite.

4. CONCLUSIONS

A generalized crystallography structural investigation of the fluorinated aluminophosphate aluminum cloverite has been presented, which goes beyond the description of the periodic aluminophosphate network. By using NMR crystallography,[59−62] simple rules that describe the nonperiodic subnetworks (i.e., the F atoms and the templates) have indeed been drawn out. Multinuclear high-resolution 1D ^{27}Al and ^{31}P NMR results are in agreement with the main topological features previously proposed for aluminum cloverite from powder X-ray diffraction, close to that of the gallophosphate cloverite. The spatial proximities extracted from the 2D $^{31}P-^{31}P$ and $^{27}Al-^{31}P$ NMR spectra of DNL-1 have allowed a full assignment of the ^{31}P and ^{27}Al resonances to the corresponding phosphorus and aluminum sites in the structure. To go beyond the description of the main framework, ^{13}C and ^{15}N NMR spectroscopy has been employed to characterize the two costructural-directing agents. The results indicate that the ethyl-methyl-imidazolium cations occupy two well-defined crystallographically inequivalent positions, while the hexa-methylen-diamine molecules are randomly distributed in the pores. This latter nonperiodic localization of the templates create a distribution of environments around the P and Al atoms, which results in the broad lines observed on the ^{31}P and ^{27}Al NMR spectra. ^1H 1D and 2D $^1H-^1H$ and $^1H-^{31}P$ NMR data have also shown that the HDA molecules are selectively in the spherical *LTA*-pores, while the $[emim]^+$ cations are found in both the *LTA*-pores and in the empty space at the intersection of the channels. Finally, the second nonperiodic subnetwork, that of the fluorine atoms, has been characterized by means of ^{19}F-X (X = ^{27}Al and ^{31}P) 2D NMR experiments. Two kinds of fluorine atoms have been distinguished: F^- ions trapped in some of *D4R* units and F atoms covalently bonded to terminal Al or P atoms and which interrupt the AlPO network. The experiments indicate that the F atoms that terminate the framework prevent the trapping of F^- ions in the terminal *D4R* cage.

Through the example of aluminum cloverite, we have shown that, despite the considerable complexity of such systems, an extremely fine level of accuracy can be reached in the structural description by coupling powder X-ray diffraction and high-resolution NMR data in a SMARTER (SMARTER stands for structure elucidation by combining magnetic resonance, computation modeling and diffractions) crystallography approach. Beyond this, the fact that the frameworks of the two studied samples DNL-1 and LUH-2 are very similar, though the samples were synthesized using different routes, clearly indicates some degree of order, which obey simple rules as described above, in the nonperiodic part of the materials and not a statistical behavior. Such an NMR crystallography study therefore represents a step toward a better understanding of the key steps in the crystal formation of porous solids.

■ ASSOCIATED CONTENT

Supporting Information. PRXD diagrams and ^1H and ^{27}Al MAS NMR spectra of the DNL-1 and LUH-2 samples prior and after overnight drying and ^{27}Al 3QMAS and parameters used for the reconstruction of the spectrum. This material is available free of charge via the Internet at http://pubs.acs.org.

■ AUTHOR INFORMATION

Corresponding Author

*Fax: +33139254476. E-mail: charlotte.martineau@chimie.uvsq.fr.

■ REFERENCES

(1) Wilson, S. T.; Lok, B. M.; Messina, C. A.; Cannan, T. R.; Flanigen, E. M. *J. Am. Chem. Soc.* **1982**, *104*, 1146–1147.
(2) Wilson, S. T.; Lok, B. M.; Flanigen, E. M. U.S. Patent 4,310,440, 1982.
(3) Lok, B. M.; Messina, C. A.; Patton, R. L.; Gajek, R. T.; Cannan, T. R.; Flanigen, E. M. *J. Am. Chem. Soc.* **1984**, *106*, 6092–6093.
(4) Lok, B. M.; Messina, C. A.; Patton, R. L.; Gajek, R. T.; Cannan, T. R.; Flanigen, E. M. U.S. Patent 4,440,871, 1984.
(5) Davis, M. E. *Nature* **2002**, *417*, 813–821.
(6) Corma, A. *J. Catal.* **2003**, *216*, 298–312.
(7) Patarin, J.; Paillaud, J. L.; Kessler, H. In *Handbook of Porous Solids*; Schuth, F. Sing, K. S. W., Weitkamp, J., Eds.; Wiley-VCH: New York, 2002; p 815.
(8) Estermann, M.; McCusker, L. B.; Baerlocher, C.; Merrouche, A.; Kessler, H. *Nature* **1991**, *352*, 320–323.
(9) Merrouche, A.; Patarin, J.; Kessler, H.; Soulard, M.; Delmotte, L.; Guth, J.-L.; Joly, J.-F. *Zeolites* **1992**, *12*, 226–232.

(10) Baerlocher, C.; McCusker, L. B.; Olson, D. H. *Atlas of Zeolites Framework Types*, 6th ed.; Elsevier: Amsterdam, 2007. See also: http://www.iza-structure.org/databases/ (accessed August 2007).
(11) Wei, Y.; Tian, Z.; Gies, H.; Xu, R.; Ma, H.; Pei, R.; Zhang, W.; Xu, Y.; Wang, L.; Li, K.; Wang, B.; Wen, G.; Lin, L. *Angew. Chem., Int. Ed.* **2010**, *49*, 5367–5370.
(12) Taulelle, F.; Pruski, M.; Amoureux, J. P.; Lang, D.; Bailly, A.; Huguenard, C.; Haouas, M.; Gerardin, C.; Loiseau, T.; Férey, G. *J. Am. Chem. Soc.* **1999**, *121*, 12148–12153.
(13) Kongshaug, K. O.; Fjellvag, H.; Lillerud, K. P. *Microporous Mesoporous Mater.* **2000**, *38*, 311–321.
(14) Kongshaug, K. O.; Fjellvag, H.; Lillerud, K. P. *Chem. Mater.* **2000**, *12*, 1095–1099.
(15) Fjellvag, H.; Akporiaye, D. R.; Halvorsen, E. N.; Karlson, A.; Kongshaug, K. O.; Lillerud, K. P. *Solid State Sci.* **2001**, *2*, 603–611.
(16) Mali, G.; Meden, A.; Ristic, A.; Tusar, N. N.; Kaucic, V. *J. Phys. Chem. B* **2002**, *106*, 63–69.
(17) Mali, G.; Rajic, N.; Logar, N. Z.; Kaucic, V. *J. Phys. Chem. B* **2003**, *107*, 1286–1292.
(18) Zhang, M.; Zhou, D.; Li, J. Y.; Yu, J. H.; Xu, J.; Deng, F.; Li, G. H.; Xu, R. R. *Inorg. Chem.* **2007**, *46*, 136–140.
(19) Kennedy, G. J.; Wiench, J. W.; Pruski, M. *Solid State Nucl. Magn. Reson.* **2008**, *33*, 76–81.
(20) Ashbrook, S. E.; Cutajar, M.; Pickard, C. J.; Walton, R. I.; Wimperis, S. *Phys. Chem. Chem. Phys.* **2008**, *10*, 5754–5764.
(21) Morais, C. M.; Montouillout, V.; Deschamp, M.; Iuga, D.; Fayon, F.; Paz, F. A. A.; Roch., J.; Fernandez, C.; Massiot, D. *Magn. Reson. Chem.* **2009**, *47*, 942–947.
(22) Ashbrook, S. E.; Cutajar, M.; Griffin, J. M.; Lethbridge, Z. A. D.; Walton, R. I.; Wimperis, S. *J. Phys. Chem. C* **2009**, *113*, 10780–10789.
(23) Yan, Z.; Chen, B.; Huang, Y. *Solid State Nucl. Magn. Reson.* **2009**, *35*, 49–60.
(24) Han, Z. X.; Picone, A. L.; Slawin, A. M. Z.; Seymour, V. R.; Ashbrook, S. E.; Zhou, W. Z.; Thompson, S. P.; Parker, J. E.; Wright, P. A. *Chem. Mater.* **2010**, *22*, 338–346.
(25) Castro, M.; Seymour, V. R.; Carnevale, D.; Griffin, J. M.; Ashbrook, S. E.; Wright, P. A.; Apperley, D. C.; Parker, J. E.; Thompson, S. P.; Fecant, A.; Bats, N. *J. Phys. Chem. C* **2010**, *114*, 12698–12710.
(26) Dedecek, J.; Lucero, M. J.; Li, C. B.; Gaon, F.; Klein, P.; Urbanova, M.; Tvaruzkova, Z.; Sazama, P.; Sklenak, S. *J. Phys. Chem. C* **2011**, *115*, 11056–11064.
(27) Martineau, C.; Mellot-Draznieks, C.; Taulelle, F. *Phys. Chem. Chem. Phys.* **2011**, *13*, 18078–18087.
(28) Chen, B.; Huang, Y. *Microporous Mesoporous Mater.* **2011**, *143*, 14–21.
(29) MacKay, A. L. *J. Mol. Struct.* **1995**, *336*, 293–303.
(30) MacKay, A. L. *Struct. Chem.* **1995**, *13*, 215–220.
(31) MacKay, A. L. *Comp. Maths Appl.* **1986**, *12*, 21–37.
(32) Martineau, C.; Engelke, F.; Taulelle, F. *J. Magn. Reson.* **2011**, *212*, 311–319.
(33) Schaefer, J.; Stejskal, E. O. *J. Am. Chem. Soc.* **1976**, *89*, 1031–1032.
(34) Pines, A.; Gibby, M. G.; Waugh, J. S. *J. Chem. Phys.* **1972**, *56*, 1776–1777.
(35) Metz, G.; Wu, X.; Smith, S. O. *J. Magn. Reson. A* **1993**, *110*, 219–227.
(36) Hartmann, S. R.; Hahn, E. L. *Phys. Rev.* **1962**, *128*, 2042–2053.
(37) Fung, B. M.; Khitrin, A. K.; Ermolaev, K. *J. Magn. Reson.* **2000**, *142*, 97–101.
(38) Amoureux, J. P.; Fernandez, C.; Steuernagel, S. *J. Magn. Reson.* **1996**, *123*, 116–118.
(39) Ernst, R.; Bodenhausen, G.; Wokaun, A. *Principles of Nuclear Magnetic Resonance in One and Two Dimensions*; Oxford University Press: New York, 1987.
(40) Hohwy, M.; Jakobsen, H. J.; Eden, M.; Levitt, M. H.; Nielsen, N. C. *J. Chem. Phys.* **1998**, *108*, 2686–2694.
(41) Ernst, R. R.; Bodenhausen, G.; Wokaun, A. *Principles of Nuclear Magnetic Resonance in One and Two Dimensions*; Clarendon Press: Oxford, U.K., 1987.
(42) Fayon, F.; King, I. J.; Harris, R. K.; Gover, R. K. B.; Evans, J. S. O.; Massiot, D. *Chem. Mater.* **2003**, *15*, 2234–2239.
(43) Sun, W.; Stephen, J. T.; Potter, L. D.; Wu, I. *J. Magn. Reson.* **1995**, *116*, 181–188.
(44) Vega, A. J. *Solid State Nucl. Magn. Reson.* **1992**, *1*, 17–32.
(45) Vega, A. J. *J. Magn. Reson.* **1992**, *96*, 50–68.
(46) Feike, M.; Demco, D. E.; Graf, R.; Gottwald, J.; Hafner, S.; Spiess, H. W. *J. Magn. Reson.* **1996**, *122*, 214–221.
(47) States, D.; Haberkorn, R.; Ruben, D. *J. Magn. Reson.* **1982**, *48*, 286–292.
(48) Hayashi, S.; Hayamizu, K. *Bull. Chem. Soc. Jpn.* **1991**, *64*, 688–690.
(49) Massiot, D.; Fayon, F.; Capron, M.; King, I.; Le Calvé, S.; Alonso, B.; Durand, J. O.; Bujoli, B.; Gan, Z.; Hoatson, G. *Magn. Reson. Chem.* **2002**, *40*, 70–76.
(50) Massiot, D.; Bessada, C.; Coutures, J.-P.; Taulelle, F. *J. Magn. Reson.* **1990**, *90*, 231–242.
(51) Blackwell, C. S.; Patton, R. L. *J. Phys. Chem.* **1984**, *88*, 61356139.
(52) Sierra, L.; Deroche, C.; Gies, H.; Guth, J. L. *Microporous Mater.* **1994**, *3*, 29–38.
(53) Brown, S. P.; Schnell, I.; Brand, J. D.; Müllen, K.; Spiess, H. W. *Phys. Chem. Chem. Phys.* **2000**, *2*, 1735–1745.
(54) Goward, G. R.; Schuster, M. F. H.; Sebastiani, D.; Schnell, I.; Spiess, H. W. *J. Phys. Chem. C* **2002**, *106*, 9322–9334.
(55) Martineau, C.; Fayon, F.; Suchomel, M. R.; Allix, M.; Massiot, D.; Taulelle, F. *Inorg. Chem.* **2011**, *50*, 2644–2653.
(56) Chott-Darie, C. S.; Patarin, J.; Le Goff, P. Y.; Kessler, H.; Benazzi, E. *Microporous Mater.* **1994**, *3*, 123–132.
(57) Schreyeck, L.; Caullet, P.; Mougenel, J. C.; Patarin, J.; Paillaud, J. L. *Microporous Mater.* **1997**, *11*, 161–169.
(58) Taulelle, F.; Samoson, A.; Loiseau, T.; Férey, G. *J. Phys. Chem. B* **1998**, *102*, 8588–8598.
(59) Taulelle, F. *Solid State Sci.* **2004**, *6*, 1053–1057.
(60) Harris, R. K. *Solid State Sci.* **2004**, *6*, 1025–1037.
(61) Taulelle, F. *Fundamental Principles of NMR Crystallography in NMR Crystallography*; Harris, R. K., Wasylishen, R., Duer, M., Eds.; J. Wiley & Sons Ltd.: Chichester, UK, 2009; p 245.
(62) Elena, B.; Pintacuda, G.; Mifsud, N.; Emsley, L. *J. Am. Chem. Soc.* **2006**, *128*, 9555–9560.